International Journal of Pattern Recognition and Artificial Intelligence, Vol. 14, No. 2 (2000) pp. 167-188

A VISON BASED SYSTEM FOR OBJECT DETECTION IN UNDERWATER IMAGES

G.L. Foresti and S. Gentili

Department of Mathematics and Computer Science (DIMI)
University of Udine, Via delle Scienze 208, 33100 Udine, Italy

Abstract – In this paper, a vision-based system for underwater object detection is presented. The system is able to detect automatically a pipeline placed on the sea bottom, and some objects, e.g. trestles and anodes, placed in its neighborhoods. A color compensation procedure has been introduced in order to reduce problems connected with the light attenuation in the water. Artificial neural networks are then applied in order to classify in real-time the pixels of the input image into different classes, corresponding e.g. to different objects present in the observed scene. Geometric reasoning is applied to reduce the detection of false objects and to improve the accuracy of true detected objects. Results on real underwater images representing a pipeline structure in different scenarios are shown. Presence of seaweed and sand, different illumination conditions and water depth, different pipeline diameter and small variations of the camera tilt angle are considered to evaluate the algorithm performances.

Keywords: *Underwater images, autonomous underwater vehicles, neural networks, geometric reasoning, object detection, object classification, illumination compensation.*

1. INTRODUCTION

Most of underwater operations are performed by remote operated vehicles (ROV) driven by human operators on a support vessel. Due to the complexity of the underwater environment, these tasks are often too expensive and tedious, and require the continue attention of the human operator to maneuver the robot in murky waters and in presence of large hydrodynamic forces [9]. For this reason, in these years, an extensive research is being performed on the development of autonomous underwater vehicles (AUVs). The main tasks that these vehicles should be able to perform autonomously are operations such as visual inspection of man-made structures (e.g. pipelines [27], off-shore structures [26]), object detection (e.g. mines [6]) and/or obstacle avoidance [10]. In the recent years, optical and acoustic systems have been developed for approaching these tasks. Zingaretti [27] developed a real-time visual imaging system for

detecting and tracking an underwater pipeline by integrating data about pipeline edges positions coming from six horizontal strips in the image. Balasuriya *et al.* [2] developed a system able to recognize visual signals produced by a set of electro-luminescent panels, representing a particular command for the AUV. Several works have been developed in the field of acoustical data. Acoustic systems (e.g., short base line, ultra short base line, long base line) are generally used for AUV position determination. Nevertheless, they need to use transponder systems and do not guarantee sufficient position accuracy due to acoustic shading and multipath effects [3]. Kristensen and Vestgård developed a multi-sensor integration system to evaluate the AUV position from acoustical data [18]. Buckingham *et al.* [7] detected neoprene coated boards submerged near a pier using the environment noise in water. Interesting works on interpretation of acoustical data can be found in [16] and in [12]. Lane *et. al.* presented a system for automatic interpretation of 3D objects based on 2D image information derived from a sector-scanning sonar device [16]. The overall interpretation reaches the 86% of successful for underwater objects viewed in different conditions. Foresti *et al*. presented a real-time system for object recognition in acoustic images [12]. A 3D acoustic camera [15] is applied to generate range images of the underwater environment.

In clear water, optical sensors present some advantages with respect to the acoustical ones. First, they generate higher data rate and with better resolution, that permit operations requiring high precision and real-time performances. Moreover, many information connected with optical data, like shading, surface marking and texture, may be useful for object recognition. However, visual-based systems are dependent on noise of the underwater image acquisition process which is characterized by several mechanisms contributing to the degradation of the video signal (see Section 3).

Several methods have been developed in the recent years to avoid problems connected with underwater imaging and perform automatic inspection of underwater environments or automatic guidance of underwater vehicles. Some methods consist in creating a mosaic of photo images of the sea floor and plan the AUV trajectory in terms of a series of time-tagged station points ([10, 13, 19]). This allows the system to have a large map of the sea bottom, studying only small parts, where the image degradation is small (typically near to the AUV). The main drawback of these methods, developed for station keeping [19] and generalized for motion [21], is the large amount of data to be stored, that makes them useless for long distances motion (e.g. pipeline inspection). Moreover, as new images are added to the existing mosaic when the AUV moves away from original positions, these methods yield large overall distortions (the error tends to accumulate in the photo-mosaic as successive images are added [25]). Other studies on AUV guidance have been focalized on the texture analysis of underwater image by co-occurrence matrices [14, 22]. However, these methods require a large amount of calculation (and so, time) necessary for the determination of the co-occurrence matrices elements. Many efforts have been done also to obtain a correct trajectory of the AUV from monocular [27] [5] or stereo image sequences [28]. If the image sequence is acquired and sampled at a sufficient high frequency, small frame to frame disparities make optical flow techniques available [4]. If frame-to-frame disparities are large, a Kalman filter is often used ([20, 24]) to perform temporal integration of extracted features. However, wrong features can introduce high error rates. Recently, Fusiello *et al.* have developed an algorithm able to detect and discard automatically unreliable feature matches over a long image sequence [28].

One of the most interesting application of vision-based underwater methods is the inspection of underwater structures, in particular, pipelines [27], cables [14] or off-shore platforms [5]. Oil and gas underwater pipelines need periodic inspections to control their conditions and to prevent

damages due to fishing activity, turbulent currents and tidal abrasion. An intelligent guidance and control system can improve the accuracy of the inspection task and it can avoid problems connected with loosing of concentration of a human operator.

In this paper, a visual system based on neural networks is applied to help an AUV to perform both visual inspection and navigation tasks. In particular, the presented system has been designed to identify a pipeline structure placed on the sea bottom, detect possible obstacles (e.g. trestles) and, in order to evaluate the AUV position along the pipeline, detect and recognize some landmark objects, i.e., anodes. The main problem in underwater objects detection, especially when the object to be identified is a pipeline long tens of kilometers, is the variation of the object characteristics, that may be very different from an image to another. This is due principally to the presence of fouling that modifies both the object texture and shape and to the presence of sand and seaweed that may partially cover these objects. For this reason, two multilayer perceptrons trained by the Back Propagation method [23] (i.e. neural networks algorithms characterized by a great generalization capability) have been considered to detect respectively pipeline edges and objects. In order to determine the AUV position, information about the probability to have a particular landmark (an anode) inside an image is supplied from an off-line database. A match between the recognized anodes and their positions along the pipeline is applied to estimate the AUV position.

2. SYSTEM DESCRIPTION

Figure 1 shows a general flowchart of the proposed system. After a color compensation (see Section 3), the size of the input image is reduced to fasten the object detection process. Two new images are generated (with size reduced to 1/16 and 1/32 of the original one) and analyzed respectively by the Edge Detection module and by the Anode Detection module. A frequency filtering based on the Fast Fourier Transform (FFT) was carried out to avoid aliasing problems.

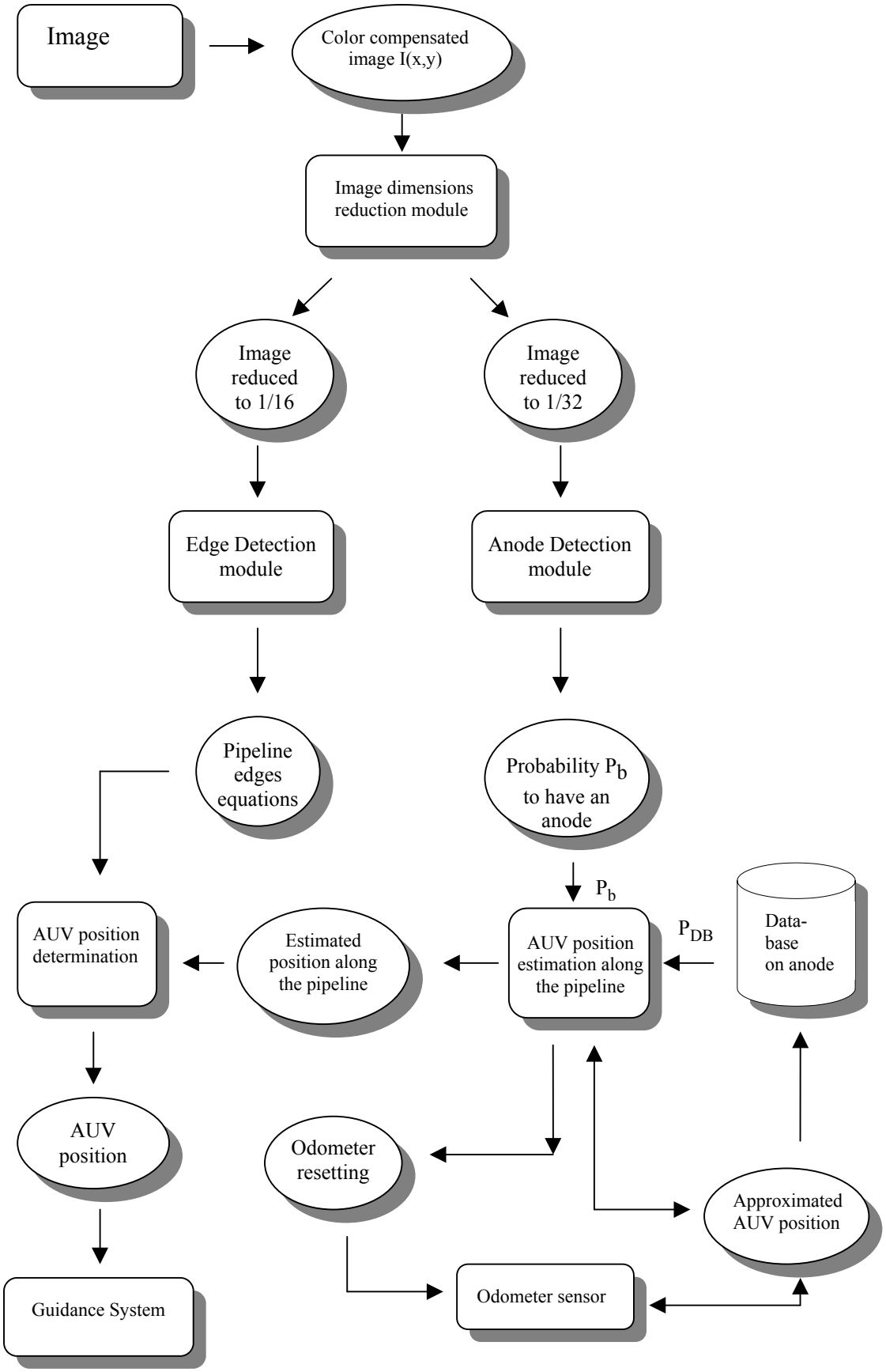

Figure 1: General flowchart of the proposed system

The Edge Detection Module (Fig. 2) uses a neural network (Fig. 3) to provide a binary classification of the input image into two classes: "pipeline edge" pixels and "background" pixels.

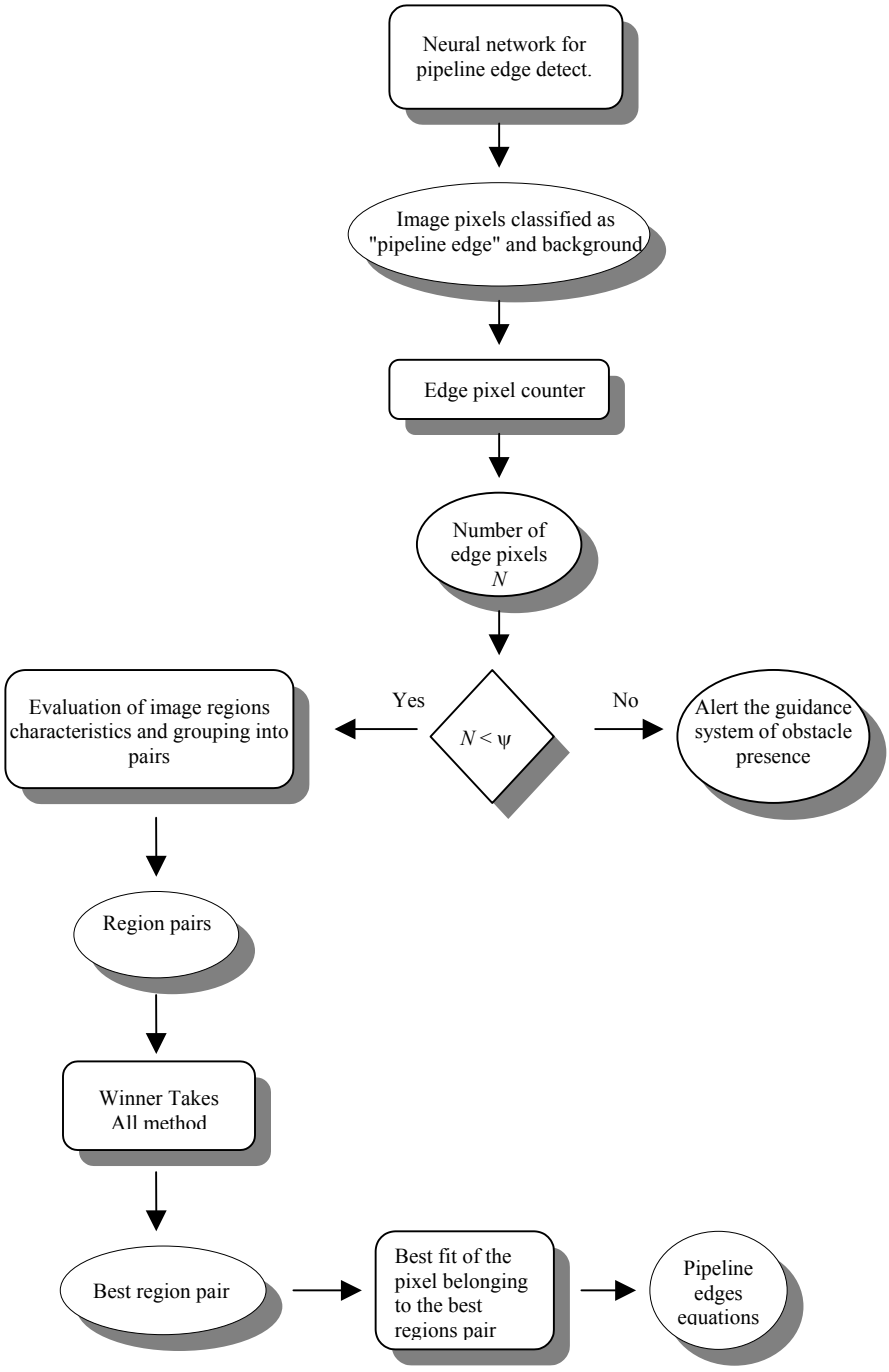

Figure2: Edge Detection Module: the module gets as input the image compensated reduced to 1/16 and returns pipeline edge equations in original image reference system.

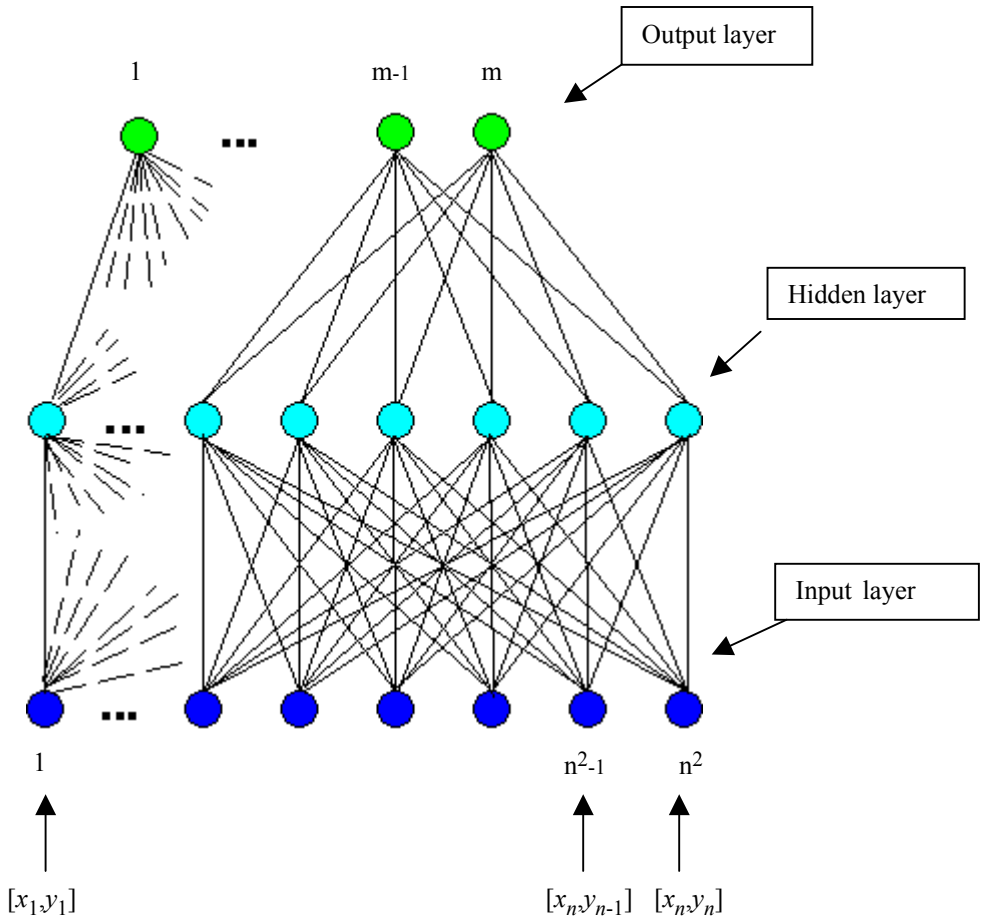

Figure 3: General scheme of a two layer applied BP model with n^2 input neurons, n^2 hidden neurons and *m* output neurons. The *nxn* sub-images to classify, are transformed into n^2 vectors and supplied as input to the neural net. The net classifies those images as belonging to one the *m* output classes.

Training patterns are extracted as *nxn* sub-images from image regions containing pipeline edges and from image regions background. The number of pixels classified as pipeline edge is counted. If it is over a given threshold ψ (depending on pipeline size and focal length and orientation of the camera), the hypothesis that an obstacle is present in the image is done, and the probability to have found the obstacle is supplied as a function of the number of pixels classified as edge. The control passes automatically to the AUV guidance system. If the number of edge pixels is under this threshold, the classification output is reconstructed as a matrix and the connected pixels are

organized into regions and then are grouped, by a geometrical reasoning method [29], into convergent pairs. A winner-takes-all mechanism is applied to find the best pair [12]. For each region pair, some characteristics as the regions area and width and the elongation of the common part of the projections of the two regions on the pair symmetry axis are extracted and analyzed, and a vote is assigned to the pair. At the end of the process, the pair with the highest number of votes is considered the winner. The best fit with a straight line is computed for each region, and the obtained coefficients are used to estimate the equations of the pipeline borders. A more detailed description of the method is presented in [11].

The Anode Detection module (see Fig. 4) uses another dedicated neural network to classify the image area included between the pipeline borders into two classes: "anode" pixels and "not anode" pixels. Analogously to the previous case, pixels classified as anode are counted, and a rough probability P_a to have an anode on the analyzed image is estimated. A test on the P_a value is performed to evaluate if the anode is present inside the image. In the affirmative case, a more accurate probability P_b to have an anode is evaluated, by considering the position of classified pixels in the output image.

To help the driving of the vehicle, an odometer evaluates roughly the position on the AUV along the pipeline. This is used to retrieve from a database containing accurate anode positions the probability P_{DB} to have or not an anode inside the image. An integration of the probabilities P_{DB} and P_b is performed to have a more accurate estimation of the AUV position along the pipeline and, if it is necessary, to perform a resetting of the odometer. The information on AUV position along the pipeline, together with the edge equations supplied by the Edge Detection module, allows to evaluate the AUV position and to guide it. When no anode is detected inside the image, the 3D position of the AUV (less accurate when the AUV is far from the anode) is supplied only by the odometer measure.

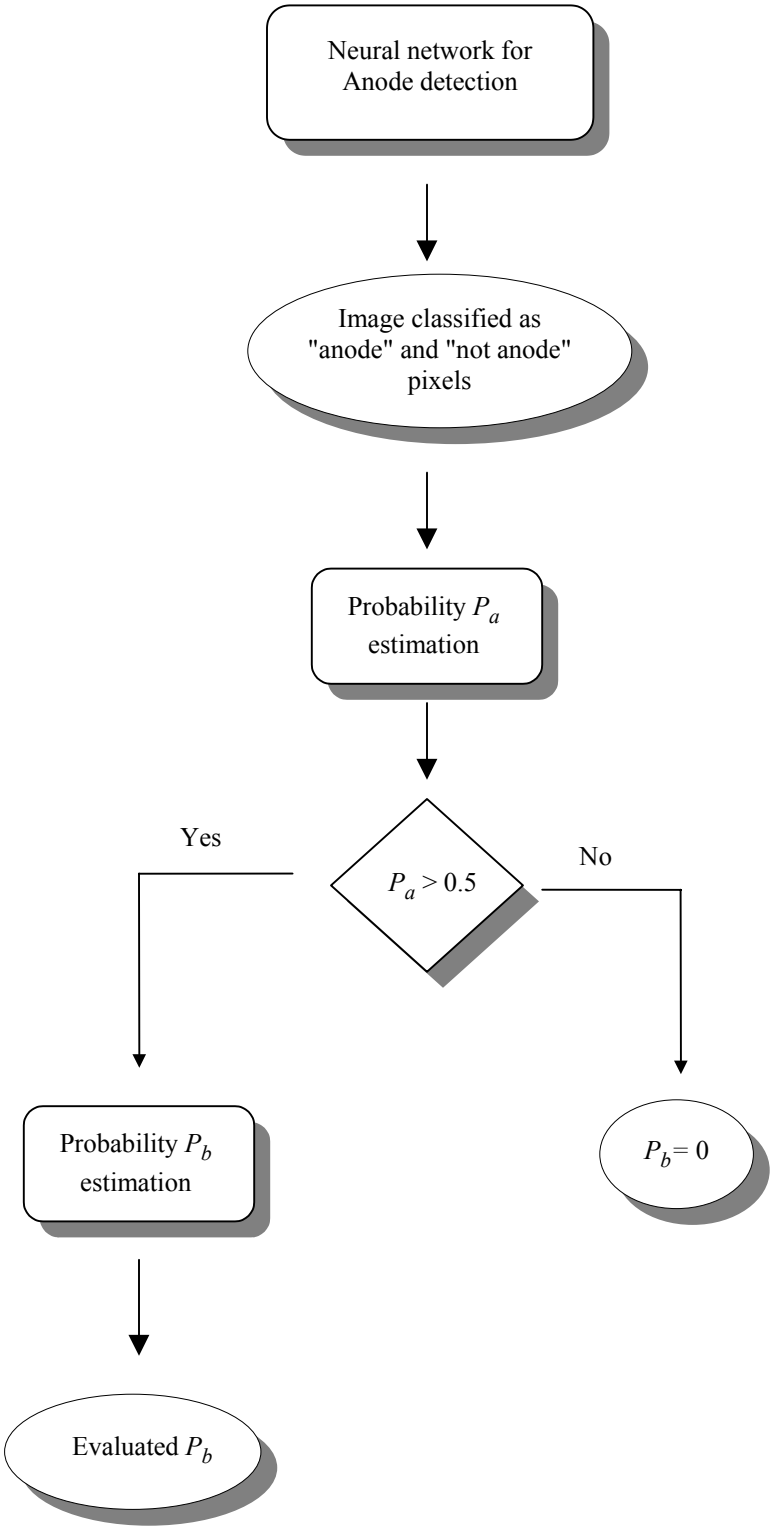

Figure 4 : Anode Detection Module: the module gets as input the image compensated reduced to 1/32 and returns the probability to have an anode inside the image.

3. ILLUMINATION COMPENSATION IN UNDERWATER IMAGES

The principal problem in underwater images analysis is the high transmission attenuation of the light through the sea water. The main causes of the attenuation are molecular scattering (the ions in the sea water increase the light scattering of about 30%), particle scattering (small pieces of organic or inorganic material held in suspension in the water can scatter light according to concentration, size distribution, water conditions and depth) and absorption (light is absorbed by the water itself and also the organic matter dissolved in it) that all contribute to the degradation of the underwater image [17,8].

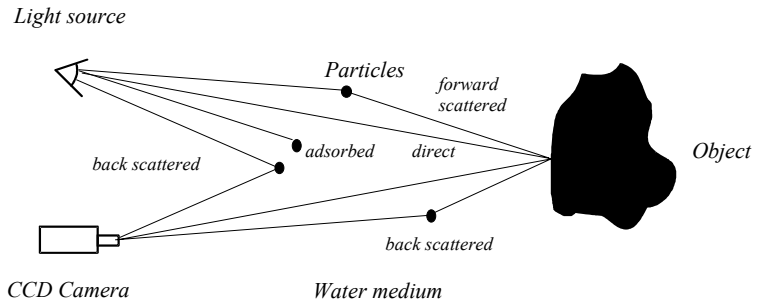

(a)

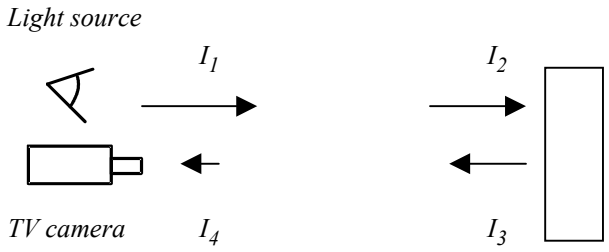

(b)

Figure 5 : (a) The main causes of attenuation of the light in water. (b) The original intensity I_1 of the incident wave is reduced near the target to $I_2 < I1$, due to the attenuation of the medium. The reflected wave of intensity $I_3 < I_2$, passing again through the medium, is attenuated, and reaches the camera with intensity $I_4 < I_3$.

The absorption process converts the light energy in other forms, essentially heat, or photosynthesis. The scattering process does not convert the light energy in other forms, but re-distributes the light spatially, causing an attenuation of the signal (see Fig. 5*a*). Absorption and scattering depend on light wavelength λ, so that underwater images need a color compensation, because some colors are more attenuated than others [8].

Due to light scattering and adsorption, the intensity I of a plane light wave passing through a medium decreases in the following way:

$$I = I_0 e^{-(\mu+h)r} \tag{1}$$

where I_0 is the intensity of the incident wave, μ is the adsorption coefficient, h the extinction coefficient (connected with the scattering process) and r is the width of the medium. The two coefficients μ and h depend respectively on the inverse of the wavelength λ and on the fourth potency of the wavelength λ; moreover, both coefficients depend on the complex refraction index n^* which has a complex dependence on λ.

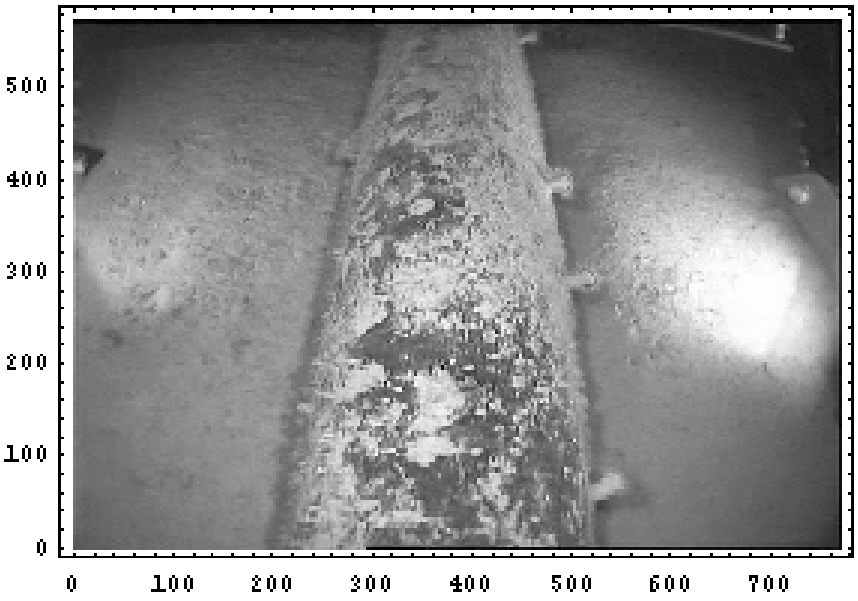

Figure 6 : An example of an underwater image representing a pipeline. Spots of light on sea bottom may be recognized as real objects inside the scene.

In underwater imaging, the problem is complicated by the artificial illumination, so that the scene is not uniformly illuminated due to a light source placed generally near to the camera. This implies that objects far from the AUV receive less light than nearer ones due to signal attenuation, and a smaller part of the reflected light is received by the camera, due to the second passage through the attenuating medium (Fig. 5*b*). Moreover, collimated AUV illuminators can cause spots of light on sea bottom that may be recognized as real objects inside the scene (see e.g. Fig. 6). Neural networks can in some cases recognize the edges of these spots as something different from pipeline borders.

The underwater image quality depends also on the response curve of the camera, that may be different from one color to another. Even if the Grey-level images are used, the color compensation is necessary, as the Grey level is defined as:

$$Grey = c_1 \,\mathrm{Re}\, d + c_2 Green + c_3 Blue \tag{2}$$

where *Red, Green* and *Blue* are the RGB components of the image, and c_1, c_2 and c_3 are chosen respectively equal to 0.3, 0.6, 0.1. As too many variables of the system are uncertain, we suppose (accordingly to equation (1)) that the attenuation law per unit (one pixel) area of the signal is given by:

$$\phi = \phi_0 e^{-\alpha d} \tag{3}$$

where α is a variable depending on the channel (R or G or B) of the image, ϕ_0 is the intensity of the incident wave per unit area and ϕ the attenuated intensity. In this approximation, the attenuation law $1/r^2$ of the flux can be neglected [17,8], because the exponential part prevails.

The main problem in image color compensation is that it is necessary to perform the correction before the 3D reconstruction of the scene, in order to have better results in edge or objects detection. This means that the distance of object from the light source must be evaluated in the image reference system, that is a projection of the real one. However, from the geometry of the

system, we evaluate that if we consider the light as coming from the bottom of the image and distance *d* as the *y* position in the image reference system, this approximation would affect principally lateral pixels on the top of the image, whose distance is under-estimated. These pixels, however, are usually very far from the pipeline, that should be maintained by the guidance system of the AUV in the central part of the image (see Fig. 7) and a under-estimation of those pixels values would not affect the system.

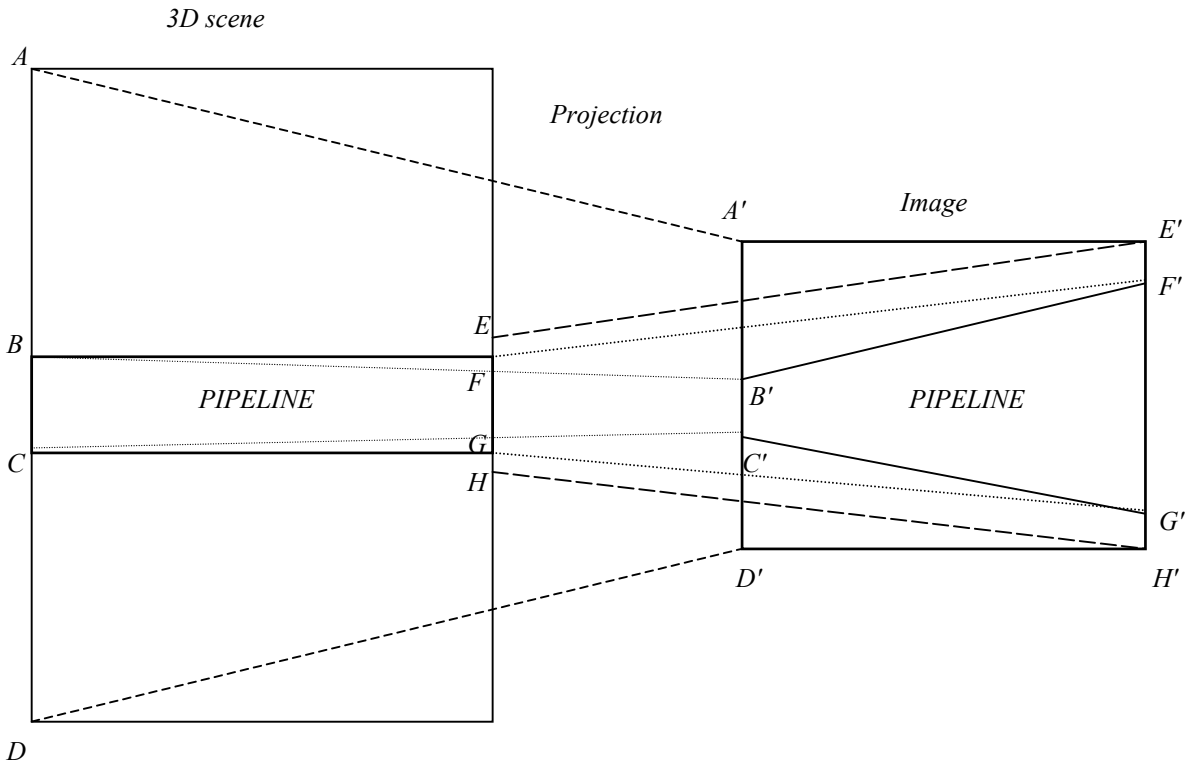

Figure 7 : Transformation of a 3D scene (on the left, seen from the top) into the 2D image registered by the camera. (on the right); points corresponding to the ones of the 3D scene are reported on the projection with the apex.

To evaluate the attenuation coefficients α_R, $\alpha_{G,}$ α_B for the R, G, B components of the image, 100 pairs of 10*x*10 (pixels) sub-images with approximately the same spectrum and intensity have been analyzed. For each pair of sub-images, the following system has been solved:

$$\begin{cases} \phi = \phi_0 e^{-\alpha d} \\ \phi' = \phi_0 e^{-\alpha d'} \end{cases} \tag{4}$$

where d and d' are the y position (in pixels) of the center of the two sub-images (see Fig.8), ϕ and ϕ' are the mean values of the sub-images pixels for every component of the image and ϕ_0 the mean value that the region should have if it was in y=0 position. The attenuation coefficients α_R, α_G, α_B have been evaluated as the median of the deduced values for the 100 sub-images pairs.

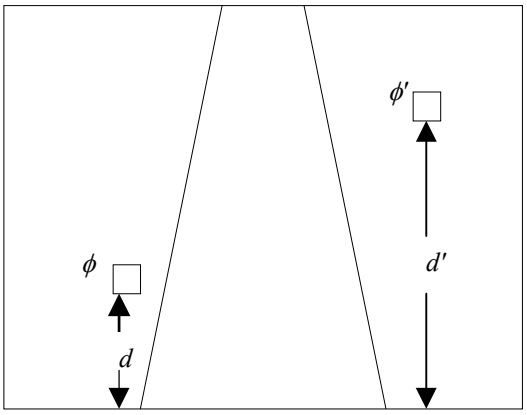

Figure 8 : 10*x*10 pixels sub-images with approximately the same spectrum and intensity, taken in different parts of the image.

To compensate the colors, it is necessary to have an equal attenuation law for all the channels. The average value in the Green channel of a pixel distant d from image bottom is:

$$\phi_G = \phi_{0G} e^{-\alpha_G d} \tag{5}$$

where ϕ_{0G} is the average value of the pixel if d=0 and ϕ_G is the measured average value. In order to have the same attenuation of the Red component also for the Green one, the following value is assigned to the pixels:

$$\phi_G' = \phi_{0G} e^{-\alpha_R d} = \frac{\phi_G}{e^{-\alpha_G d}} e^{-\alpha_R d} = \phi_G e^{-(\alpha_R - \alpha_G) d} \tag{6}$$

Analogously, the following new value is assigned to the Blue component of the pixel:

$$\phi_B' = \phi_B e^{-(\alpha_R - \alpha_B)d} \quad (7)$$

where ϕ_B the measured pixel value and ϕ_B' the corrected one.

As the attenuation law is the same for all channels into the corrected image, a correction of the Grey-scale image could be easily performed by multiplying the pixel values by the term $e^{\alpha_R d}$. However, this compensation would not recover the information on texture and contrast lost due to bad illumination of images regions far from the light source. As the proposed system is more sensitive to shape (e.g. sea bottom-pipeline, edge-pipeline) than to intensity, this correction has not been considered.

Figure 9 shows a general flowchart of the color compensation method, while in Fig. 10 an example of color compensation is presented.

4. UNDERWATER OBJECTS DETECTION

In order to accomplish the AUV navigation task, it is necessary to detect the presence of objects along the pipeline, for two different reasons:

(a) obstacle avoidance (detection must be done in real-time, to permit to the AUV to change its direction); trestles represent the more frequent obstacles that can be found along a pipeline;

(b) if the position of some particular objects (*landmarks*) is well known, it is possible to validate the AUV position by integrating information about the detected objects with a database containing object positions along the pipeline and information on the AUV position supplied by an odometer; anodes represent possible landmarks.

A. Trestles detection

Trestles are very tall objects used to keep the pipeline close to the sea bottom. They are characterized by four legs driven into the ground and four legs in the opposite direction, used to put the trestle in the right position (see Fig. 11a). As they are tall objects, their detection is

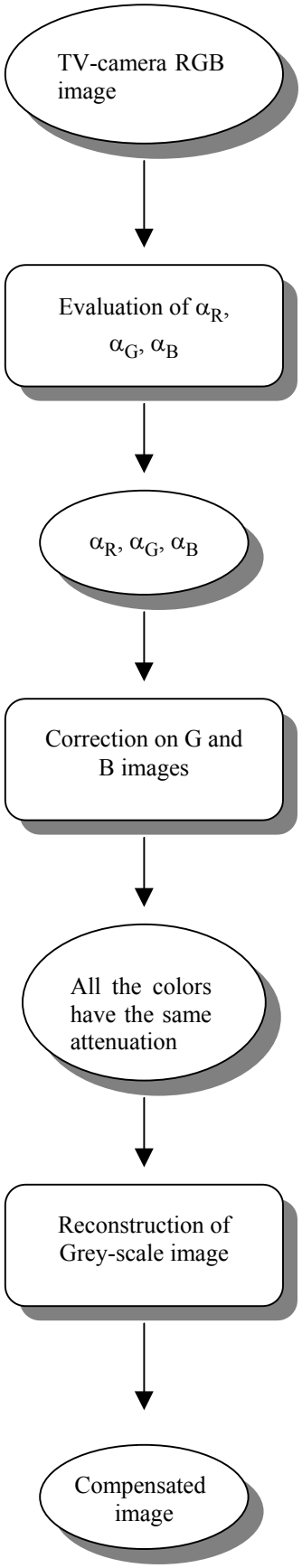

Figure 9 : General flowchart of the of the color compensation method.

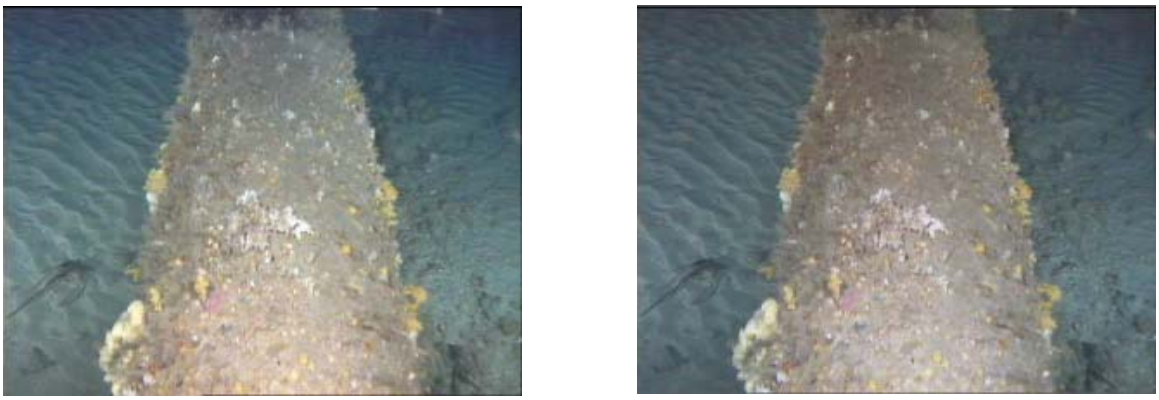

(a) (b)

Figure 10 : An example of color compensation for an underwater image representing a pipeline; (a) original image, (b) compensated image.

necessary during the AUV navigation to avoid collisions. Generally, the image which contains such objects is extremely complex, and, it is really difficult to apply a classical object recognition method to identify trestles. However, if an image contains a trestle, a great number of pixels is classified as edge by the neural network trained to detect pipeline edges. Therefore, it is possible to detect their presence only by verify that the number of pixels classified as edges is greater than a given threshold. Figure 11b shows the obtained classification on the image in Fig. 11a. A probability function to be near to an obstacle like a trestle can be obtained as:

$$\begin{cases} P_T = \dfrac{n-\psi}{\Phi-\psi} & n > \psi \\ 0 & otherwise \end{cases} \tag{8}$$

where n is number of pixels classified as edge in the analyzed image, Φ is the maximum number of pixels classified as edges on a long test image sequence and ψ is the maximum number of pixels classified as edge in an image in which there is no trestle.

B. Anodes detection

Anodes are added to the pipeline to avoid corrosions due to the photoelectric effect. Due to the

existence of different anode types, i.e., characterized by different materials and different shapes, it is complex to learn a neural network to classify all different types of anodes as the same object.

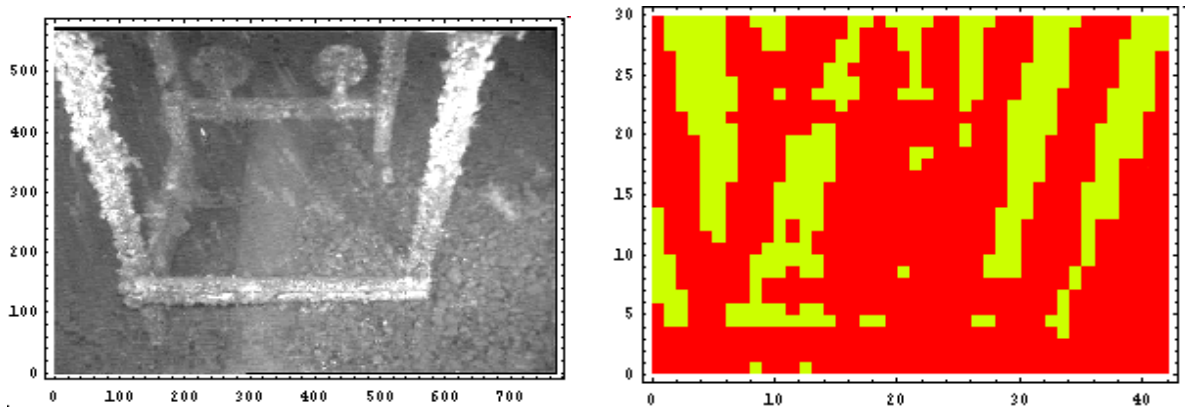

(a) (b)

Figure 11: (a) An example of a trestle object, (b) edge detection by applying neural network to image in Fig 11a.

Some examples of anodes are presented in Fig. 12. For anode detection, a more specialized neural network, trained by Back Propagation method, has been developed. Like in the edge detection case, it is necessary to perform an image reduction to avoid too long processing times.

(a) (b) (c)

Figure 12: (a) An anode on a pipeline covered by *gunite*. There is a small difference of intensity from the anode and the pipeline itself and no difference between the anode radius and the pipeline radius. (b) The *gunite* is not covering the pipeline. The intensity difference is greater than in the previous case and there is a difference between the pipeline and the anode radius. (c) The AUV is approaching the anode and consequently only a part of it can be seen.

In particular, the input image, after a color compensation, is reduced to 1/32 of the original image. Unlike the previous case, the neural network learning was made by patterns of size 17*x*17 pixels, and two classes are chosen: *anode* and *not anode*. Anode learning patterns contain

examples of different kind of anodes. If the anode is present in the image, at least 70% of the pixels are classified as "anode", otherwise, if there is no anode, less than 10% of the pixels are classified as "anode", even if in the most cases they are exactly 0. A rough probability to have an anode in a given image is obtained as:

$$P_a = \frac{n_a}{N} \tag{9}$$

where n_a is the number of pixels classified as anode in the considered image and N is the total number of pixels in the same image. If the anode dimensions are small, it may happen that only a part of pixels are classified as anode, even if the anode presence is absolutely certain, i.e., probability equal to 1. In these cases, we obtain a value of P_a belonging to the range (0.7,1). For this reason, a more accurate probability P_b is computed. Let r be the radius of the anode that can be estimated as:

$$r = \sqrt{\frac{\sum (\boldsymbol{a}_i - \boldsymbol{c})^2}{n_a}} \tag{10}$$

where $\boldsymbol{a}_i = (a_x, a_y)_i$ is the position of each pixel classified as anode and $\boldsymbol{c}$ is the barycentre of the anode defined as:

$$\boldsymbol{c} = \frac{\sum \boldsymbol{a}_i}{n_a} \tag{11}$$

The probability P_b to have an anode is then estimated as:

$$P_b = \frac{N_p}{N_T} \tag{12}$$

where N_p is the number of pixels classified as anode inside a circle of radius *r* with center coincident with the barycentre of the anode and N_T is the total number of pixels inside that circle. In this way,

(a) if $N_p = N_T \Rightarrow P_b = 1$,

(b) if $N_p = 0 \Rightarrow P_b = 0$

(c) for every N_p, $P_b \propto N_p$.

For the anodes presented in Fig. 12, the probabilities P_a are respectively 0.94, 0,75 and 0,56, while probabilities P_b are all equal to one.

C. AUV position determination

The AUV position is measured by an odometer which produces an error that increases as the AUV goes away from the last known position. This error is due principally to the presence of currents that do not permit to the AUV a rectilinear and uniform motion. Landmark detection can be used to obtain an estimate of the AUV position along the pipeline. The system resets automatically the odometer sensor when the probability P_{NN} to have found an anode given by the neural network is over a threshold and the match with the database is positive.

Let us suppose that the probability density function $f(\gamma)$ of the error γ on the AUV position along the pipeline is a Gaussian function centered on the last known position s_0, i.e.,

$$f(\gamma) = \frac{1}{\sqrt{2\sigma_\gamma^2}} e^{-\frac{(\gamma - s_0)^2}{2\sigma_\gamma^2}} \tag{13}$$

Let S be a 1D reference system with origin in s_0 (position of the last detected landmark) and orientation coincident with that of the pipeline (Figure 13). Let s be the real coordinate of the AUV and $\hat{s}$ the measured one.

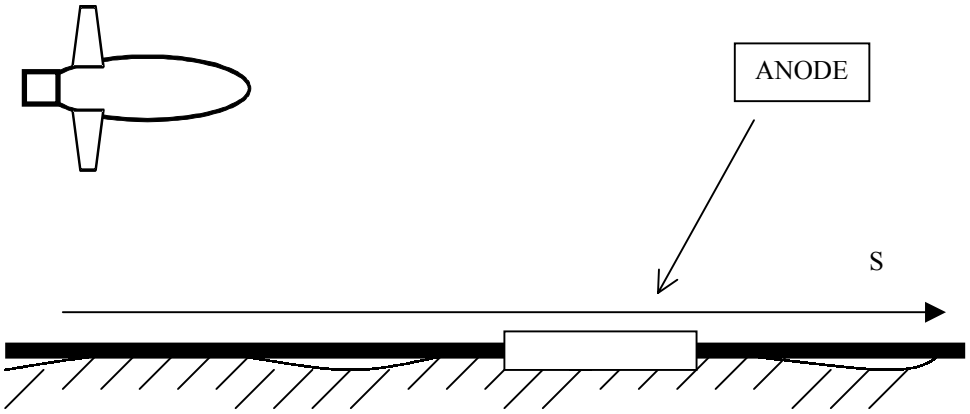

Figure 13: AUV motion along the pipeline. S is the real coordinate of the AUV and $\hat{S}$ the measured one.

The real position of the AUV is given by $s = \hat{s} \pm \gamma$, so the distribution of s will be :

$$f(s) = \frac{1}{\sqrt{2\sigma_\gamma^2}} e^{-\frac{(S-\hat{S}\pm\gamma)^2}{2\sigma_\gamma^2}} \tag{14}$$

As σ_γ is time-varying, it is useful to reset the AUV position measure frequently as possible, to avoid too large errors in s estimation. The match between the Anode Detection Module, the odometer information on AUV position and a database containing precise anode positions along the pipeline, can be useful to deduce exact position of the AUV along the pipeline and reset the measures of the odometer sensor. Let s_k be position of the k-th landmark. The probability that the AUV has passed the point s_k is given by:

$$P(s \geq s_k / \hat{s}) = 1 - P(s \leq s_k / \hat{s}) = 1 - \int_{-\infty}^{s_k} f(s)ds \tag{15}$$

Information about $P(s \geq s_k / \hat{s})$ can be used to activate the neural network to search for landmarks only when the probability that the AUV is near to a landmark is high, e.g., the measures of the odometer sensor are reset when $P(s \geq s_k / \hat{s}) > 0.9$. Finally, from equations (14) and (15), it possible to obtain:

$$P(S \geq S_0 / \hat{S}) = 1 - P(S \leq S_0 / \hat{S}) = 1 - \int_{-\infty}^{S_0} \frac{1}{\sqrt{2\sigma_\gamma^2}} e^{-\frac{(s - \hat{s} \pm \bar{\gamma})^2}{2\sigma_\gamma^2}} dS \tag{16}$$

and by putting $t = S - \hat{S}$, the equation (16) becomes :

$$P(S \geq S_0) = 1 - P(S \leq S_0) = 1 - \int_{-\infty}^{S_0 - \hat{S}} \frac{1}{\sqrt{2\sigma_\gamma^2}} e^{-\frac{(t \pm \bar{\gamma})^2}{2\sigma_\gamma^2}} dt \tag{17}$$

so that, from the equation $P(S \leq S_0) \geq 0.9$ it is possible to numerically evaluate $\hat{S}$.

5. RESULTS

The presented system is able to find pipeline edges and other objects, e.g., anodes and trestles, in different underwater environments. A set of about 800 real underwater images has been considered as test set. The time necessary to our system to process an image (by a C language program on a 200MHz Pentium Pro computer) is about 1.5 seconds.

A. Pipeline edge detection

Figure 14 shows the estimated pipeline edges for different kind of pipelines. Fig. 14a represents a pipeline placed on a sea bottom characterized by sand and seaweed. The presence of seaweed and darker sand on the right side of the image causes a little angle error in best fit line.

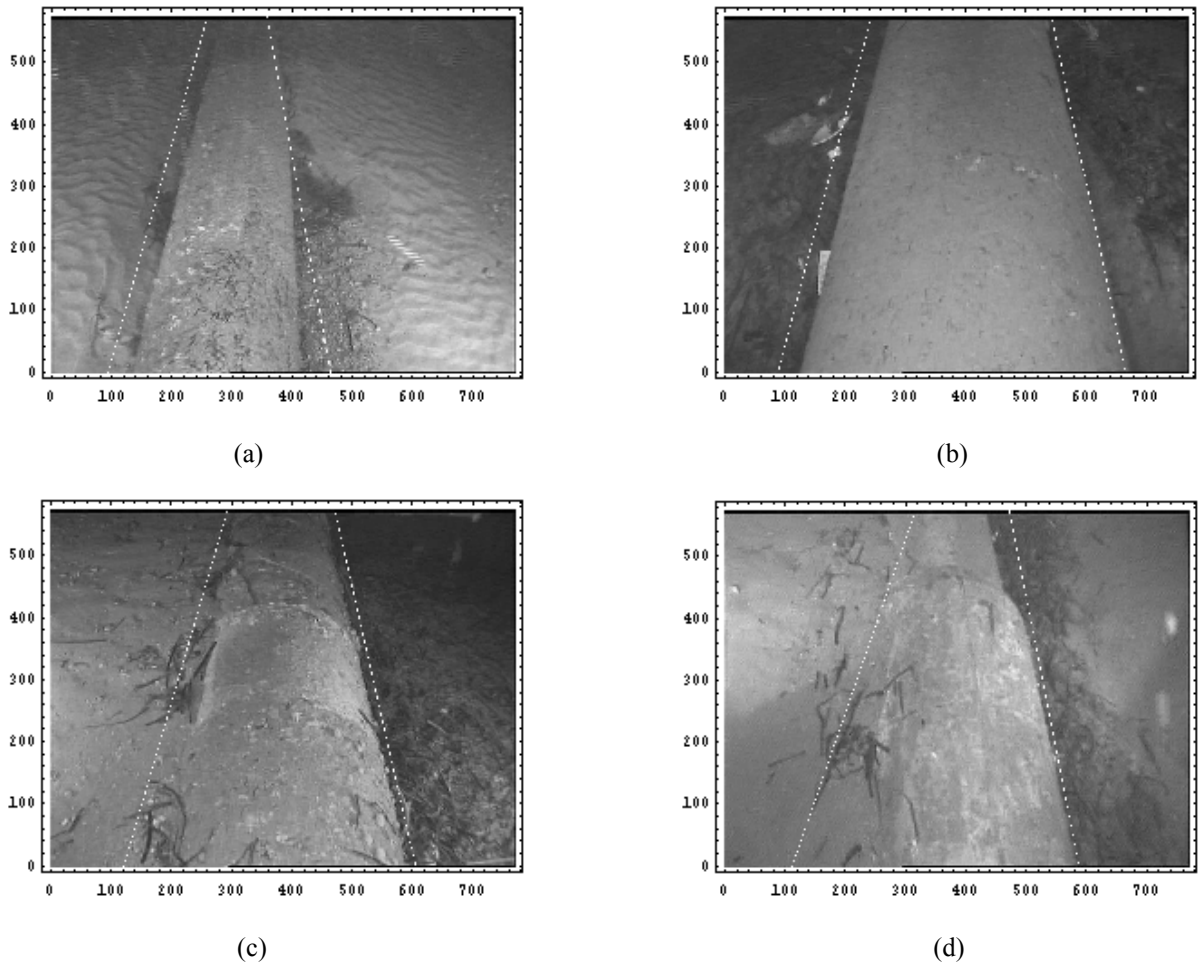

Figure 14 : Some results of the pipeline edge extraction algorithm on different real situations : (a) pipeline on sand and seaweed, (b) pipeline on seaweed, (c) pipeline partially covered by sand.
(d) pipeline with a border completely covered by sand.

The seaweed on left side causes a small translation in edge position due to widening of the classified region. Fig. 14b represents a pipeline on seaweed with some debris on the right side. This fact causes a small translation of left edge. The most interesting scenario is shown in Fig. 14c. It represents a typical situation in pipeline inspection: the pipeline is partially covered by sand on one (left) edge. Also in this situation, the edge is correctly detected on the basis of the different texture of the pipeline and the sand. In all three cases, edges are found with a good

approximation, i.e., the minimum square error on the edge position is 0.87, 0.97 and 0.94, respectively. The errors are usually only on one edge and in presence of sand totally covering an edge (Fig. 14d). It is important to notice that anyway at least one of the two edges is found with a good approximation. The robustness of the object detection procedure have been estimated by means of the three measures introduced by Algar and Theil [1]: *precision (P)*, *recall (R)* and *goodness (G)*. Let $e = e_T + e_F$ be the total number of detected pipeline edges, e_T is the number of true detected edges and e_F is the number of false detections. Let E be the total number of edges on the test set of 700 images. Precision, recall and goodness are defined respectively as ratios :

$$P = \frac{e_T}{e} \tag{18a}$$

$$R = \frac{e_T}{E} \tag{18b}$$

$$G = \frac{e_T - e_F}{E} \tag{18c}$$

The procedure is robust when all these ratios are close to one. On a test set of 700 images, the following values have been found: P=0.93 , R=0.96 and G=0.89, so the proposed method can be considered enough robust to solve the problem of pipeline edge detection in underwater images.

B. Anode detection

The proposed algorithm for underwater object detection has been tested on a set of 100 images: 50 images containing anodes and 50 without anodes. The first test has been performed on images containing only anodes. The algorithm found anodes in the 95% of the input images; moreover, on test set of 50 images which do not contain anodes, no anode has been detected.

Like for pipeline edge detection, the P, R and G values ($P = \frac{a_T}{a}, R = \frac{a_T}{A}, G = \frac{a_T - a_F}{A}$) have been computed, where $a = a_T + a_F$ is the total number of detected anodes, a_T is the number of detected anodes on images containing an anode, a_F is the number of detected on images without anodes and A is the total number of anodes on the test set of 100 images. The following values have been found $P=1$, $R=G=0.95$ as $a_F = 0$, which demonstrate the robustness of the proposed method.

C. Trestles detection

In order to evaluate the probability to have an trestle inside the image, it is very important to evaluate correctly the values of Φ and ψ, i.e. respectively of the maximum number of pixels classified as edges in any image sequence and the maximum number of pixels classified as edge in images in which there is no trestle.

After several tests on more than 50 underwater images, the values $\Phi \cong 300$ and $\psi \cong 250$ have been found. The parameter γ, in particular, is very important as it determines if the system detects or not a trestle. There are some rare particular cases in which, due to the presence of other large objects or a lot of small objects on the sea bottom, it may happen that images without trestle present a number of pixels classified as pipeline greater or equal to some others containing a trestle. As many of those images contain other kind of obstacle (e.g. drums, garbage etc.), in order to guarantee the navigation safety, a opportune value of γ has been chosen, so that the system classifies those images as containing a trestle.

Some tests have been made on a set of 50 images containing trestles, and trestles have been detected in all cases with a probability P_T always over 0.7. However, this method depends widely on images and principally on the distance of the AUV from the trestle. A test set of 50 images

without trestles has been added to the test set and the P, R and G values ($P = \frac{t_T}{t}$, $R = \frac{t_T}{T}$, $G = \frac{t_T - t_F}{T}$) have been evaluated, where $t = t_T + t_F$ is the total number of detected trestles, t_T is the number of detected trestles in images containing a trestle, t_F is the number of detected trestles in images without trestles and T is the total number of trestles on the whole test set. The values of P, R and G result respectively 0.94, 1, 0.94.

It is important to notice that all the images, containing a lot of small objects, wrongly classified as trestles, are characterized by a very low probability, i.e., $P<0.2$.

6. CONCLUSIONS

A vision-based system for underwater object detection has been presented. This method which can be applied to AUV navigation is able to determine the edges of pipeline structure the presence of landmarks like anodes and of obstacles like trestles. A color compensation procedure aimed in order to reduce problems connected with the light attenuation in the water has been presented.

The method adopted for pipeline edge detection consists of two steps. First, a neural network is applied to segment the underwater image into different regions corresponding to pipeline edges or sea bottom; then, all the possible regions pairs are analyzed, in order to determine the right one. Satisfactory results are obtained also for pipelines partially occluded, i.e., covered by sand.

The method adopted for obstacle determination is based on the evaluation of the number of pixels classified as edge in the whole image. If this value is greater than a fixed threshold, the presence of an obstacle in the scene is hypothesized.

The method adopted to evaluate the anode presence inside the image uses a dedicated network able to classify the image in the two classes “anode” and “no anode”. If the number of pixels

classified as anode is over a given threshold, the algorithm passes to evaluate classified image characteristics in order to evaluate the probability to have an anode inside the image. A method to evaluate AUV position from a matching between this probability and the probability supplied by a database is presented .

Experimental results show how the presence of seaweed and sand, different illumination conditions and water depth, different pipeline diameter and small variations of the tilt angle of the camera do not affect too much the algorithm performances.

REFERENCES

1. V.S. Alagar and L.H. Thiel, "Algorithms for Detecting *M*-Dimensional Objects in *N*-Dimensional Spaces", *IEEE Transactions on Pattern Analysis And Machine Intelligence* **3** (1981) 245-256.
2. B.A.A.P. Balasuriya, T.Fujii and T.Ura, "A Vision Based Interactive System for Underwater Robots" in Proc. of IEEE IROS '95, Pennsylvania, 1995, pp. 561-566.
3. B.A.A.P. Balasuriya, T. Fujii and T. Ura, "Underwater pattern observation for positioning and communication of AUVS", *Proc. of IEEE IROS '96*, 1996, pp. 193-201.
4. J.L.Barron, D. J. Fleet and S. Beauchemin, "Performance of optical flow techniques", *International Journal of Computer Vision*, **9** (1994) pp. 43-77.
5. A. Branca, E. Stella and A. Distante, "Autonomous navigation of underwater vehicles", in Proc. of *Oceans '98*, Nice,France, 1998 pp. 61-65.
6. D. Brutzmann, M. Burns, M. Campbell, D.Davis, T. Healey, M. Holden, B.Leonhardt, D.Marco, D.McLarin, B. McGhee and R. Whalen "NPS Phoenix AUV Software Integration and In-Water Testing", in Proc. of *IEEE Autonomous Underwater Vehicles (AUV) 96*, Monterey, California, 1996, pp. 99-108.
7. M.J. Buckingham, B. V. Berkout and A.A.L.Glegg, "Imaging the ocean ambient noise" , *Nature*, **356** (1992) pp. 327-329.
8. S.Q. Duntley, "Light in the sea" *Journal of the Optical Society of America* **53** 1963.
9. Davies R. S. "Remote Visual Inspection in nuclear, pipeline and underwater industries" *Materials evolution*, Vol 48, (1990) 797-803.
10. S. D. Fleischer and S. M. Rock. "Experimental Validation of a Real-Time Vision Sensor and Navigation System for Intelligent Underwater Vehicles. " Proc of *IEEE Conference on Intelligent Vehicles*, Stuttgart, Germany, 1998.

11. G.L. Foresti, S. Gentili and M. Zampato “Autonomous underwater vehicle guidance by integrating neural networks and geometrical reasoning*”, International Journal of Imaging Systems and Technology* (in press).
12. G.L.Foresti, V.Murino, C.S.Regazzoni and A.Trucco, “A Voting-Based Approach for Fast Object Recognition in Underwater Acoustic Images”, *IEEE Journal of Oceanic Engineering* **22** (1997) 57-65.
13. N. Gracias and J.Santos-Victor "Automatic Mosaic Creation of the Ocean Floor", in Proc of *Oceans '98*, Nice, France, 1998, pp. 257-262.
14. A. Grau, J. Climent and J. Aranda "Real-time architecture for cable tracking using texture descriptors", in Proc. of *Oceans '98*, Nice,France, 1998, pp. 1496-1500.
15. R.K.Hansen, P.A.Andersen, "3D Acoustic Camera for Underwater Imaging", *Acoustical Imaging* **20** (1993) pp. 723-727.
16. D.M. Lane and J.P. Stoner, "Automatic interpretation of sonar imagery using qualitative feature matching" IEEE Journal of Oceanic Engineering, **19** (1994) pp. 391-405.
17. N.G. Jerlov, *Marine Optics*, Elsevier Oceanography Series, No.14, Amsterdam, 1976.
18. J.Kristensen and K. Vestgård "Hugin - An Untethered Underwater Vehicle for Seabed Surveying", Proc of *Oceans '98*, Nice, France, 1998, pp. 118-123.
19. R. L. Marks, S. M. Rock and M. J. Lee "Real-Time Video Mosaicking of the Ocean Floor" *IEEE Journal of Oceanic Engineering* **20** (1995) pp. 229-241.
20. L. Matthies, T. Kanade and R. Szelinsky, "Kalman filter based on algorithms for estimating depth from image sequencies", *International Journal of Computer Vision* **3** (1989) pp. 209-236.
21. S. Negahdaripour, X. Xu an A. Khamene "Application of Direct 3D Motion Estimation of Underwater Machine Vision Systems" Proc of *Oceans '98*, Nice, France, 1998, pp. 51-55.
22. T.R. Reed and J. M. Hand du Buf "A review of recent texture segmentation and feature extraction techniques" *Computer Vision Graphics and Image Processing: Image Understanding* **57** (1993) pp. 359-372.
23. B.D. Ripley, Pattern recognition and neural networks, *Cambridge University Press*, 1996.
24. L. S. Shapiro, H. Wang and J.M. Brady "A matching and tracking strategy for independently moving objects", in Proc. of *British Machine Vision Conference* 1992 pp. 306-315.
25. H. Singh, J. Howland, D. Yoerger "Quantitative Photomosaicing of Underwater Imaginery" in Proc of *Oceans '98*, Nice, France, 1998, pp. 263-266.
26. J.S.Smith, R.Yu, I.Sarafis, J.Lucas, "Computer Vision Control of an Underwater Manipulator", in Proc. of *OCEANS 94*, Brest, Sept. 1994, Vol. I, pp. 187-192.
27. G. Tascini, P. Zingaretti, and G.P Conte "Real-Time Inspection by Submarine Images", *Journal of Electronic Imaging*, **5**, 1996, pp.432-442.

28. T. Tommasini, A. Fusiello, E. Trucco, and V. Roberto. "Making good features track better", in Proc. of *IEEE Conference on Computer Vision and Pattern Recognition*, Santa Barbara, CA, 1998 pp. 178-183.
29. E.L.Walker, and M.Herman, “Geometric Reasoning for constructing 3D scene descriptions from images”, in *Geometric Reasoning*, (D.Kapur, J.Mundy, eds), MIT Press, 1989, pp.275-290.